PCCP

Accepted Manuscript

ROYAL SOCIETY OF CHEMISTRY

www.rsc.org/pccp

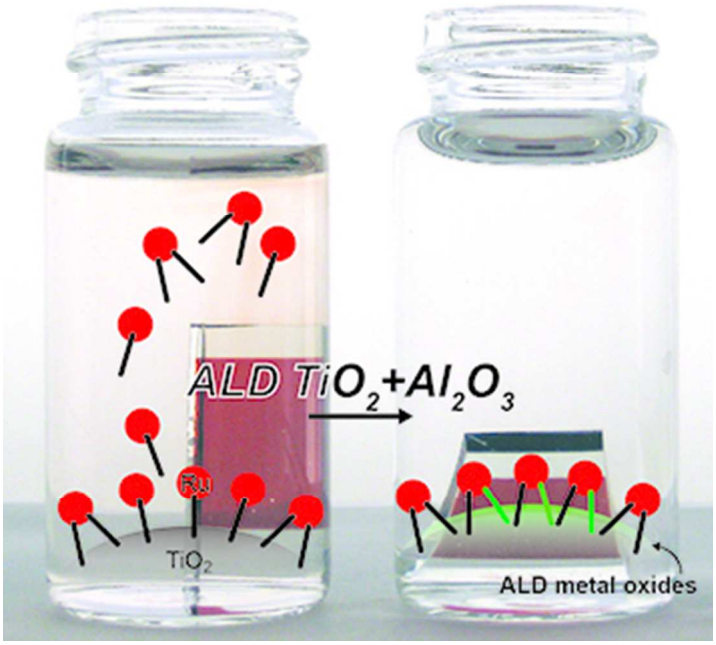

49x49mm (180 x 180 DPI)

PCCP

RSCPublishing

ARTICLE

Stabilizing chromophore binding on TiO_2 for long-term stability of dye-sensitized solar cells using multicomponent atomic layer deposition

Cite this: DOI: 10.1039/x0xx00000x

Received 00th January 2012,
Accepted 00th January 2012

DOI: 10.1039/x0xx00000x

www.rsc.org/

Do Han Kim[a], Mark D. Losego[a], Kenneth Hanson[b], Leila Alibabaei[b], Kyoungmi Lee[a], Thomas J. Meyer[b], and Gregory N. Parsons[a*]

Ambient humidity and high temperature are known to degrade dye-sensitized solar cells (DSSCs) via chromophore desorption. Recently, enhanced dye-attachment to TiO_2 surfaces has been realized by coating molecularly functionalized surfaces with inorganic atomic layer deposition (ALD) coatings. Here, we apply this ALD approach to DSSCs and demonstrate that high energy conversion efficiencies can be maintained while significantly extending device lifetimes. While single component ALD layers show improved high-temperature stability, it significantly degraded up to 45% of initial DSSC performance right after ALD. We, however, find that mixed component ALD layers provide initial efficiencies within 90% of their untreated counterparts while still extending device lifetimes. Optimized ALD protection schemes maintain 80% of their initial efficiency after 500 h of thermal aging at 80 °C whereas efficiency of DSSCs with no ALD protection drop below 60% of their initial efficiencies. IR spectroscopy conducted *in situ* during ALD reveals that carboxylate linker groups transition from unbound or weakly-bound states, respectively, to more strongly bound bidentate structures. This strategy to improve dye-attachment by ALD while maintaining high performance is novel and promising for extending the functional lifetime for DSSCs and other related devices.

1. Introduction

While dye-sensitized solar cells (DSSCs) have achieved power conversion efficiencies at costs that allow them to compete economically with more traditional semiconductor photovoltaics, their interface complexity introduces challenges to achieve the long-term stability necessary for large-scale commercialization.[1–3] DSSCs are generally composed of molecular chromophores (sensitizers) attached to a conductive inorganic nanostructure with high surface area (e.g., mesoporous TiO_2). The molecular sensitizers absorb solar radiation and generate excited electrons that are injected into the inorganic scaffold. The electrical circuit is completed via immersion of the nanostructure in an electrolyte with a redox couple. The complex tandem interactions between nanostructure, molecular sensitizer, and electrolyte introduces a number of mechanisms for device failure and reduced lifetime.[4] Common mechanisms of short lifetime include evaporation of the electrolyte, detachment of the sensitizers via hydrolytic attack by water, or sensitizer degradation by UV-illumination.[5] Engineering "impermeable" sealants has been the primary approach for extending DSSC lifetime.[3,5] While this approach impedes the penetration of external contaminants, it provides no inherent protection to the complex device structure. Thus, devices are still susceptible to detrimental species introduced by side reactions between dye, electrolyte, and TiO_2 that lead to dye-detachment when exposed to high temperature, UV-light, or small amounts of oxygen.[6–8]

Several approaches for inherently stabilizing molecular sensitizers have been applied with limited success. One approach is to use amphiphilic dyes with hydrophobic moieties that repel water combining with hydrophilic groups that strongly bind to the inorganic nanostructure's surface.[9,10] A second approach is to kinetically impede dye-desorption via the addition of co-adsorbents under temperature control or the addition of excess dye to the electrolyte.[11–13] Recently, Park et al. have used *in situ* cross-linking polymerization to physically immobilize dye molecules on a TiO_2 surface.[14] In this polymer membrane method, a steric acid monolayer co-adsorbed with N719 improved dye stability in DSSCs under thermal stress at T< 65 °C. Stability is known to be strongly temperature dependent, and 80 °C where our tests are performed is particularly demanding.[3,10,14–16]

Moreover, the oligomer adsorption requires wet processing steps which are energy- and solution-intensive. In contrast, dry vapor processes do not require drying steps and produce less waste.

Herein, we demonstrate that vapor-phase atomic layer deposition (ALD) of subnanometer layers composed of inorganic materials applied after dye-sensitization improves dye-attachment and reduces DSSC sensitivity to both moisture and temperature. Atomic layer deposition uses sequential, self-limited surface reactions to enable subnanometer film thickness precision and exquisite conformality over complex three-dimensional nanostructures.[17] Therefore, a number of previous reports have demonstrated that ALD on mesoporous structure of DSSCs prior to dye-sensitization can improve DSSC performance. For example, ALD coated nanostructures have shown reduced recombination of photo-excited carriers with core-shell structures.[18–21] ALD layers have been also used as blocking layers at the collector electrode.[22]

Although recent investigations in our lab have shown improved dye-attachment using either Al_2O_3 or TiO_2 for ALD, clear questions about potential device performance were raised due to reduced charge injection rates in ultrafast spectroscopy experiments.[23,24] Multicomponent ALD layers may help avoid losses by optimizing chemical attachment and electronic band structure at the electrolyte contact. Herein, we provide a novel study to directly address device performance by fabricating and testing full DSSCs with a commercial N719 dye integrated with multicomponent ALD binding layers. We find that the ALD stabilization layers with specific cycle ratio of two components modestly degrade the initial DSSC performance, but after aging for 500 h at 80 °C in dark, devices with the ALD layers show efficiencies markedly higher than control DSSCs aged under the same conditions. Interfacial bonding between dye and mesoporous TiO_2 (meso-TiO_2) is observed during ALD process using *in situ* Fourier transform infrared spectroscopy (FTIR) to further elucidate the mechanisms of improved performance.

2. Experimental

2.1. Preparation of dye-sensitized photoanodes

Meso-TiO_2 photoanodes were prepared on FTO glass (TEC 8, Pilkington). Prior to preparation, a 5 nm TiO_2 blocking layer was deposited onto the FTO glass by ALD at 150°C and then annealed at 500°C for 30 min in air.[22] Meso-TiO_2 was fabricated by spreading TiO_2 paste (d = 20 nm, Ti-Nanoxide H/SP, Solaronix) over the TiO_2 blocking layer with 3M Scotch tape™ as a spacer. These structures were then calcinated at 500°C for 30 min to remove organic binders of the paste. After annealing, the TiO_2 layer measured 6 µm thick. This coating process was repeated three times to achieve a total meso-TiO_2 thick of 18 µm. A light scattering layer composed of large TiO_2 particles (d=100 nm, Ti-Nanoxide R/SP, Solaronix) was then added on the top. These meso-TiO_2 electrodes were next sensitized in an anhydrous ethanol solution of 0.5 mM N719 dye (cis-diisothiocyanato-bis(2,2'-bipyridyl-4,4'-dicarboxylato) ruthenium(II) bis(tetrabutylammonium), N719, Solaronix) for 24 h at room temperature. After sensitizing, the photoanodes were washed with anhydrous ethanol to remove excess dye molecules and dried with a nitrogen gas stream.

2.2. Atomic layer deposition on dyed meso-TiO_2

A homemade viscous-flow ALD reactor was utilized to deposit Al_2O_3 and TiO_2 at 70°C and 1 Torr flowing ultra-pure nitrogen carrier gas (99.999%, National welders). Al_2O_3 layers were synthesized using sequential doses of trimetylaluminum (TMA, Strem) and H_2O while TiO_2 was synthesized from titanium tetrachloride ($TiCl_4$, Strem) and H_2O. Prior to deposition, photoanodes were held in the reactor at 70°C for 30 min in flowing dry nitrogen to remove adsorbed moisture on meso-TiO_2. For better coverage, precursors were commonly dosed for 1 s, held for 15 s, and purged for 90 s. Holds were done by closing a gate valve in front of the pump.

2.3. Dye desorption test

Dye desorption tests were carried out on 6 µm thick meso-TiO_2 layers. The first desorption test was conducted in aqueous basic 1 mM KOH solution (pH 10). The another desorption experiment used the standard iodine / triiodide electrolyte contaminated with 5 vol% deionized water. Electrolyte composition was the same as DSSCs fabrication: 0.7 M 1-butyl-3-methylimidazolium iodide (BMII), 0.03 M I_2, 0.1 M guanidinium thiocyanate (GSCN), and 0.5 M 4-tert-butylpyridine (TBP) in mixture of acetonitrile and valeronitrile with a volume ratio of 85:15. In both experiments, dye-desorption was performed in independent vials, at room temperature, and in the dark. UV-vis spectrum were timely measured after rinsing with anhydrous ethanol and drying with nitrogen.

2.4. DSSC fabrication

A Pt cathode with drilled holes was prepared by solution casting and pyrolyzing a 7 mM H_2PtCl_4 isopropanol solution on a clean FTO-glass substrate. The FTO glass was treated by air-plasma to improve wetting property of Pt precursor. A few drops of the platinum solution were drop cast off on the FTO glass, and then annealed at 500 °C for 30 min in air. The Pt cathode was immediately assembled with a photoanode using 60 µm thick Surlyn® sheet as a gasket. Electrolyte was filled in the void space between the two electrodes using a syringe. The holes were then sealed with a Surlyn® sheet and micro-slide glass.

2.5. Thermal aging test

After keeping DSSCs in the dark at room temperature for three days to fully infiltrate meso-TiO_2 with electrolyte, they were moved to a dark furnace for thermal aging at 80°C. DSSCs were cooled to room temperature before each measurement.

2.6. *In situ* IR spectroscopy

Spectrum were obtained using a Nicolet 670 Thermo Scientific spectrometer integrated with a home-built ALD reactor as described in our prior report.[25] Each spectrum was acquired from a total of 2050 scans with a resolution of 4 cm^{-1}. Only for IR measurement 6 µm thick meso-TiO_2 films on double side-polished Si was made by identical method to DSSC photoanode fabrication procedures.

2.7. Incident photon-to-conversion efficiency (IPCE)

IPCE values were obtained by using a 75W Xe Oriel 6251 / Oriel Cornerstone 260 monochromator from which light was coupled through an optical fiber and made incident on to the DSSC setup. Incident light intensity measurements were done by using a calibrated Si-photodiode.

2.8. Transient absorption (TA) spectroscopy

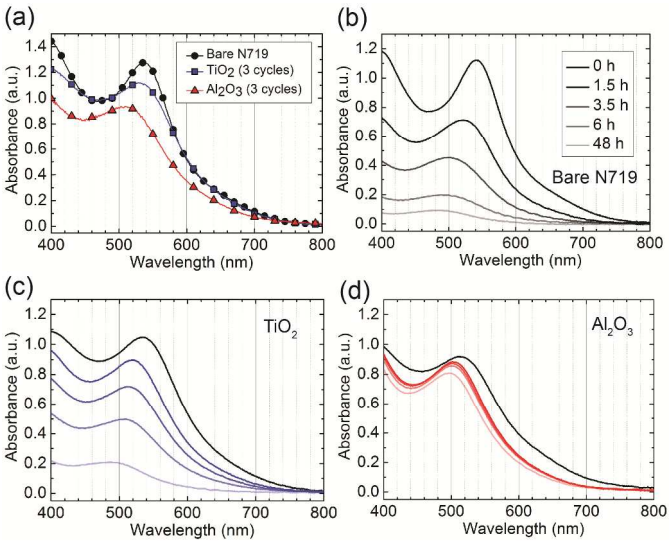

Figure 1. UV-vis absorbance change of TiO_2–N719 (a) before and after ALD, UV-vis spectra change during dye-desorption in KOH solution with (b) untreated TiO_2-N719 and treated TiO_2-N719 with (c) TiO_2 ALD, (d) Al_2O_3 ALD

TA measurements were carried out by inserting derivatized thin films at a 45° angle into a standard 10 mm path length square cuvette containing acetonitrile with 1 M $LiClO_4$. The top of the cuvette was fit with an O-ring seal with a Kontes valve inlet to allow the contents to be purged with Argon. TA experiments were performed by using nanosecond laser pulses produced by a Spectra-Physics Quanta-Ray Lab-170 Nd:YAG laser combined with a VersaScan OPO (532 nm, 5-7 ns, operated at 1 Hz, beam diameter 0.5 cm, ~5 mJ/pulse) integrated into a commercially available Edinburgh LP920 laser flash photolysis spectrometer system. White light probe pulses generated by a pulsed 450 W Xe lamp were passed through the electrode, focused into the spectrometer (at 500 nm with 3 nm bandwidth), then detected by a photomultiplier tube (Hamamatsu R928). A 532 nm notch filter was placed before the detector to reject unwanted scattered light. Detector outputs were processed using a Tektronix TDS3032C Digital phosphor oscilloscope interfaced to a PC running Edinburgh's L900 (version 7.0) software package. Single wavelength kinetic data were the result of averaging 50 laser shots and were fit using the Edinburgh software. The data were fit from 50 ns to 10 μs by using the tri-exponential function in equation 1 and the weighted average lifetime (<τ>) calculated from equation 2.

$$y = A_1 e^{-(1/\tau_1)x} + A_2 e^{-(1/\tau_2)x} + A_3 e^{-(1/\tau_3)x} \quad (1)$$

$$\tau_i = 1/k_i \; ; \; <\tau> \; = \Sigma A_i \tau_i^2 \; / \; \Sigma A_i \tau_i \quad (2)$$

Electron injection efficiencies (Φ_{inj}) were calculated by using thin film actinometry with untreated dyed TiO_2 (TiO_2-N719) in MeCN (0.1 M $LiClO_4$) as the reference, which is known to have an injection yield of 100%.

2.9. DSSC characterization

Photocurrent–voltage (I-V) was measured using a solar simulator (M-9119, Newport) equipped with a 300 W xenon lamp and an AM 1.5G filter. A calibrated silicon-based solar cell (91150V, Newport) was used to calibrate light intensity before every measurement. A source meter (Keithley 2400) recorded the photocurrent with a sampling delay time of 40 ms. Black matte paper with suitable apertures was used to mask divergent or scattered light coming from the sides of the cell.[26] To measure the TiO_2 active area of the DSSCs, images were obtained with a digital camera (IXUS 500, Canon) and a National Institute of Standards and Technology (NIST) certified ruler. Area was evaluated with ImageJ software. All electrical data (I-V and IPCE) are obtained from three identically prepared DSSCs. The error bars represent one standard deviation.

3. Results and Discussion

3.1. Effects of ALD on the optical absorption and attachment of N719

UV-vis absorbance data in Figure 1(a) reveal spectral changes after depositing three ALD cycles of Al_2O_3 or TiO_2 onto sensitized meso-TiO_2 electrodes. Both ALD cause a blue-shift of N719's metal-to-ligand charge transfer (MLCT) band (~532 nm). The shift is somewhat larger for Al_2O_3 than TiO_2 at the same number of ALD cycles and it increases proportionally with ALD layer thickness (see Figure S1 in the supplementary information). To evaluate dye-attachment, sensitized electrodes are immersed in aqueous basic solution at pH 10 (KOH) at room temperature for 48 h. Such solutions are commonly used to strip dye molecules from oxide surfaces.[14,27] A video in the supplementary information shows significantly retarded dye desorption after applying three ALD cycles to the sensitized electrodes. Figures 1(b), (c), and (d) show the dye absorbance versus time for the control structure, ALD TiO_2 coated structure, and ALD Al_2O_3 coated structure respectively. Dye molecules desorb slowly after ALD TiO_2, whereas ALD Al_2O_3 strongly protects dye-attachment on meso-TiO_2. For comparison, Figure S2 shows the difference in desorption by plotting peak absorbance of the MLCT versus desorption time. The half decay time of TiO_2-N719 is increased to 11 h compared to 6 h for untreated TiO_2-N719. ALD Al_2O_3 shows the best dye-attachment losing only 10% of the initial MLCT absorbance after 48 hours.

3.2. *In situ* IR spectroscopy

IR spectroscopy is a useful analytical tool for investigating chemical changes to molecular chromophores used in DSSC devices. We have constructed a unique ALD reactor capable of *in*

situ transmission IR spectroscopy as described previously.[28] This *in situ* capability permits analysis during each ALD half reaction (i.e., precursor dosing and co-reactant dosing) without exposure to atmosphere. For these experiments, a double-side-polished Si wafer with resistivity of ~100 Ω is used as an IR transparent substrate. Meso-TiO_2 thick of 6 μm is screen-printed onto Si wafers and dye-sensitized in the usual way.

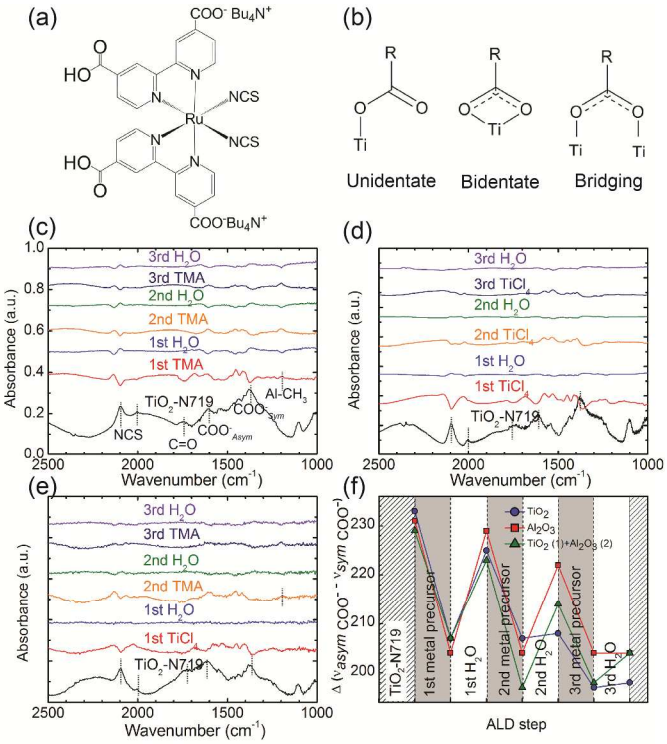

Figure 2(a) N719 dye molecule (b) Major three binding modes of N719 to meso-TiO2 (c) In situ differential FT- IR of ALD on TiO2-N719, ALD Al2O3 (three cycles) (d) ALD TiO2 (three cycles) (e) ALD TiO2 one cycle and then ALD Al2O3 two cycles (f) Difference in frequency of asymmetric COO- (1608 cm-1) and symmetric COO- (1382 cm-1) stretching modes at each ALD step.

Figure 2(a) shows molecular structure of N719, and Figure 2(b) schematically illustrates the three major surface binding modes between meso-TiO_2 and N719. Figure 2(c)-(e) summarizes the IR spectra collected during three cycles of ALD Al_2O_3, TiO_2, and Al_2O_3/TiO_2 mixed layers onto TiO_2-N719. The bottom spectrum (black) in Figure 2(c)-(e) is the initial absorbance spectrum collected from the TiO_2–N719 prior to ALD treatment. Each subsequent trace is a difference spectrum, showing the net change from the previous collected spectrum. In this way, relative absorbance changes that occur during each ALD half-cycle are highlighted. That is to say, new absorption bands produce positive-going peaks, while valleys indicate the disappearance of an absorption band.

Considering the spectra for the TiO_2–N719 known from literature, absorption peaks are observed for bound carboxylate (1382, 1608 cm^{-1}), unbound carboxylic acid (1716 cm^{-1}), and thiocyanate (2000-2050 cm^{-1}) groups.[11,14,29–31] The carbonyl peak near 1716 cm^{-1} indicates that some of the N719's carboxylic groups are either unbound or unidentate bound to the TiO_2 surface in Figure 2(b).[30,31] The first differential spectrum (red) shows that all of these modes are influenced by the first precursor exposure step. Most noteworthy is that the 1716 cm^{-1} mode disappears after a single exposure to trimethylaluminum (TMA) or $TiCl_4$. This suggests that the unbound carbonyl units react with the metal precursors, promoting extra bonds to form between N719 and the meso-TiO_2 surface. While the detailed mechanism is not rigorously identified, it is likely that the TMA or $TiCl_4$ forms a Lewis acid/base adduct with the Lewis base carbonyl group, promoting reaction during the subsequent water exposure to form oxygen-metal-oxygen linkages to the surface. Meanwhile, the mode of bound carboxylates can be further assessed by evaluating the spectral separation between asymmetric and symmetric COO^- stretches.[31,32] Spectral narrowing between the $\nu_{asym}(COO^-)$ and $\nu_{sym}(COO^-)$ absorption bands indicates a transitioning from unidentate to bidentate binding in Figure 2(b).[32] Unidentate is the weakest binding mode and the most susceptible to hydrolytic attack resulting in dye desorption, particularly at high temperatures.[5,10,33] Meantime, bidentate modes are stronger and also provide more effective charge–injection.[29,34] In Figure 2(f) we plot $\Delta\nu = \nu_{asym}(COO^-) - \nu_{sym}(COO^-)$ as a function of each ALD half cycle. For all ALD process, the spectral separation of $\nu_{asym}(COO^-)$ and $\nu_{sym}(COO^-)$ oscillates during each ALD half cycle with an overall trend of progressively decreasing spectral separation. We interpret the overall decrease in separation as an indication of more effective bidentate attachment of the N719 molecule to the inorganic scaffold. The oscillatory nature during each ALD half cycle suggests that H_2O doses may partially detach the carboxylate group to form a unidentate binding mode. This hydrolytic attack is gradually reduced as additional ALD layers are applied due to limited available reaction sites. Empirically, we observe no significant decrease in the separation after three ALD cycles. Therefore, a large number of ALD cycles is not necessary to strengthen binding modes between dye and TiO_2. Rather, too much ALD coating can clog pores of meso-TiO_2 and totally damage photophysical function of dye degrading performance.[24]

In addition to changes to the carboxylate binding mode, we also observe a systematic shift in the thiocyanate (NCS) absorption band at 2000-2050 cm^{-1} with each ALD half cycle. NCS peaks in Figure 2(c)-(f) also shift frequency, as evident in comparison with the spectrum in Figure S4. This is attributed to oxidation of the NCS by TMA or $TiCl_4$, where the nucleophilic C≡N, Lewis base sites are attacked by the Lewis acid precursors.[35] This process is at least partially reversed during the H_2O dosing step. Likely, the oxidation of the NCS group causes the blue-shift in the UV-vis absorption spectra (Figure 1a) and impacts the regeneration quantum yield of the N719 dye.[6,35]

3.3. Photophysics analysis of electron transfer kinetics

Transient absorption (TA) spectroscopy is used to assess electron injection yields (Φ_{inj}) and back electron transfer rates for TiO_2 –-N719 electrodes having total 3 ALD cycles with different sequences and results are in Table 1. Based on the measured growth per cycle and the standard deviation, all the samples in Table 1 have ~ the same thickness, within ~±1 Å. Previously, we used TA spectroscopy to examine electron injection yields for $Ru(bpy)_2(4,4'\text{-}(PO_3H_2)bpy)$ dye adsorbed on meso-TiO_2, and found that thicker ALD coatings generally decrease the total electron injection yields.[24] We find similar trends for ALD films

Table 1. Summary of electron injection yields (Φ_{inj}) measured from transient absorption with the respect to the number of ALD cycles, metal oxides, and sequences in mixture materials

Electrode			Cycle of ALD		Φ_{inj} [b]	lifetime (μs)				k_{bet} ($10^4 s^{-1}$)
			Al_2O_3	TiO_2		τ_1 (A_1)	τ_2 (A_2)	τ_3 (A_3)	$<\tau>$	
Untreated N719			0	0	1.00	0.10 (2)	0.78 (11)	9.31 (87)	9.2	10.8
ALD [a]	TiO_2 first	TAA	2	1	0.60	0.08 (4)	0.66 (19)	5.91 (77)	5.8	17.3
		TTA	1	2	0.45	0.08 (6)	0.56 (27)	3.31 (67)	3.1	32.0
		TTT	0	3	0.40	0.07 (6)	0.41 (23)	2.29 (71)	2.2	45.8
	Al_2O_3 first	ATT	1	2	0.50	0.05 (4)	0.27 (19)	1.83 (77)	1.8	56.4
		AAT	2	1	0.60	0.08 (6)	0.54 (27)	3.21 (67)	3.0	33.0
		AAA	0	3	0.55	0.07 (5)	0.52 (24)	3.73 (71)	3.6	27.9

[a] denotes ALD sequence composed of ALD TiO_2 and Al_2O_3. For example, TAA means that a cycle of TiO_2 ALD is performed on dyed TiO_2, and then two cycles of Al_2O_3 ALD are done. [b] based on TA measurement at delay time at 50 ns in 1 M $LiClO_4$ in MeCN. Full TA traces are in Figure S3.

on N719 sensitized meso-TiO_2 electrodes. Figure S5 shows the injection yield monotonically decreases after 1, 3, 5, and 10 cycles of TiO_2 or Al_2O_3.

However, the mechanism for the decline differs for TiO_2 and Al_2O.[36] Specifically, we hypothesize that Al_2O_3 layers simply act as dielectric barriers to charge transfer while TiO_2 layers increase back electron transfer rates to electrolyte in picosecond timescales that make injection yields (Φ_{inj}) appear to decrease. Based on this premise, we postulate that mixed layers of Al_2O_3 and TiO_2 ALD could potentially counterbalance one another and improve overall performance. Measured injection yields for such "bicomponent ALD layers" are summarized in Table 1. Here we use the notation of "A" to represent a single Al_2O_3 ALD cycle and "T" to represent a single TiO_2 ALD cycle. In nearly all cases, these four mixed ALD process show improved injection yields when compared to the pure component treatments (TTT and AAA), consistent with our hypothesis. We find that injection yields are highest when the Al_2O_3:TiO_2 cycle ratio is 2:1, for either titania first (TAA) or alumina first (AAT).

3.4. Optical properties and stability of bicomponent ALD layers

The bicomponent ALD layers show changes in optical properties that are consistent with trends obtained for the single component layers. For the 2:1, alumina/titania coating (TAA and AAT), the MLCT absorbance band shift is between that for the pure Al_2O_3 and that for pure TiO_2 (Figure S6). Using an acetonitrile / valeronitrile electrolyte solution containing the iodide / triiodide redox couple and 5 volume % water contamination, we tested electrode stability for 24 h in the dark at room temperature. The dye desorption was tracked using UV-vis absorbance, and results are shown in Figure 3 and S7. The untreated electrode visually shows a large loss of N719 dye, as shown in Figure 3(a). Using the full UV-vis spectrum in Figure S7, we compare the dye desorption from one uncoated and six ALD-treated electrodes. The normalized absorbance near the MLCT at 532 nm is shown for each electrode in Figure 3(b). The normalized absorbance decays biexponentially, which is consistent with dye desorption kinetics.[7] Untreated electrode exhibits very rapid desorption rates (83% loss of initial absorbance), whereas all ALD treated electrodes show much slower desorption rates (< 50%). Sensitized electrode treated with three cycles of Al_2O_3 ALD (AAA) shows the best stability (34%, loss in absorbance at MLCT) and a bicomponent ALD layer, TAA, is also very stable (39 %). Even if three ALD cycles of TiO_2 show the worst stability (59 %) among treated electrodes, it is still 40% better than the untreated electrodes. Additionally, Figure S8 confirms that electrolyte after this desorption test contains desorbed N719 dye in inverse proportion to electrode stability.

3.5. Dye-sensitized solar cells and thermal aging test

To evaluate DSSC performance and lifetime, seven separate sets of DSSCs were prepared. These sets included one control and six sets that underwent different ALD sequence, but the same number of ALD cycles, three. These six ALD treatments are same to listed in Table 1. Figure 4(a) shows initial DSSC performances measured under calibrated AM 1.5G illumination, along with standard deviation obtained from three identically prepared devices. In these measurements, the cell edge was masked to avoid lateral light effect.[26,37] The coloration in bar charts indicates compositional structure for ALD layers. While the initial conversion efficiencies for all ALD treated DSSCs are lower than the control, TAA and AAT have efficiencies within 10% of the untreated DSSC. Power conversion efficiencies generally

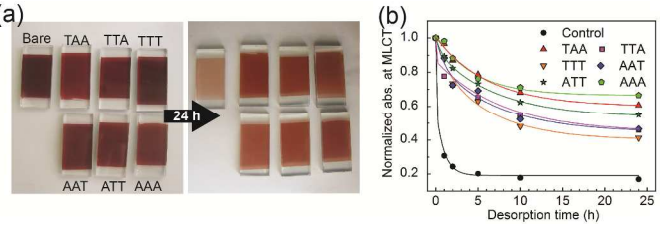

Figure 3. Dye-desorption test using water contaminated iodine-electrolyte in dark at room temperature (a) Color change of TiO_2-N719 after 24 h (b) Normalized absorbance change at MLCT of N719

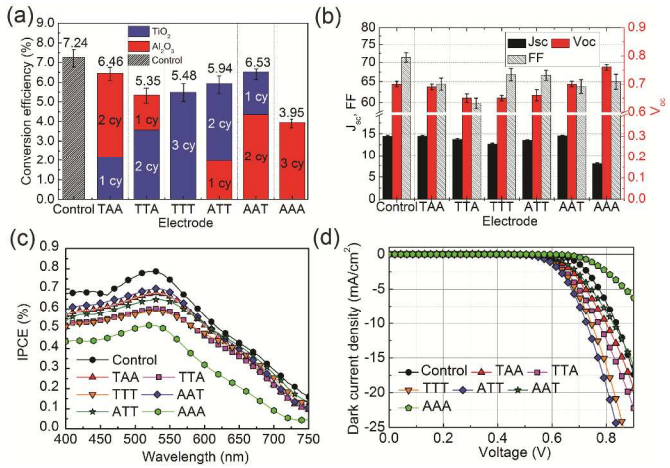

Figure 4. Initial performances of DSSCs with total three ALD cycles (a) Overall conversion efficiency (b) J_{sc}, V_{oc}, and FF obtained from each three DSSCs (c) IPCE (d) dark currents from randomly picked DSSCs

correlate with measured electron injection yields (Φ_{inj}) in Table 1 (Figure S9). As observed in the *in situ* IR analysis, the Al_2O_3 ALD coating strongly affects the NCS unit in the N719. The NCS is known to regenerate oxidized N719 through the oxidation of iodine electrolyte.[35] Therefore, the degraded performance observed in the AAA set of devices may be due to NCS modification.

Figure 4(b) shows how various device performance are affected by the ALD coatings. While the coatings appear to affect the short circuit current density (J_{sc}), open circuit voltage (V_{oc}) and fill factor (FF), the J_{sc} appears most closely correlated to conversion efficiency. We note that devices with the Al_2O_3 coating show higher V_{oc}, possibly due to interface dipoles that increase the apparent TiO_2 conduction band edge.[38,39] The improved V_{oc} is also consistent with ALD Al_2O_3 reducing the TiO_2/electrolyte interface state density. Additionally, the ALD coating may increase the device series resistance and impact the FF.

Incident photon-to-current efficiencies (IPCE) are reported in Figure 4(c). The diminished IPCE at shorter wavelengths and particularly near the MLCT absorption band of N719 (532 nm) appears to parallel UV-vis absorption data as shown in Figure 1(a) suggesting that the reduction in device efficiency is the result of decreased light absorption at shorter wavelengths. At longer wavelength region than MLCT, AAA shows the lowest IPCE different from other treated DSSCs. This again could be attributed to changes in the NCS ligand or unfavorable electronic coupling between N719 and conduction band of TiO_2.[40,41] The IPCE data also shows generally better initial performance for the electrodes with multicomponent compared to those with TiO_2 or Al_2O_3 alone.

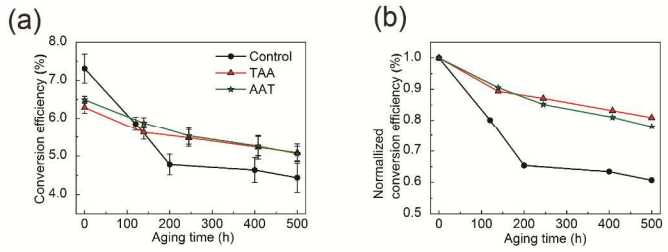

Figure 5. Thermal aging test at 80 °C in dark for 500 h (a) conversion efficiency, (b) normalized conversion efficiency of untreated and best treated DSSC. Full data with other ALD combinations are described in Figure S10 including J_{sc}, normalized J_{sc}, V_{oc}, and, fill factor (FF).

The existence of different metal oxides on the meso-TiO_2 can be validated form dark currents, and results are represented in Figure 4(d). The Al_2O_3 typically increases the barrier ability to reduce charge recombination that occurs between TiO_2-N719 and electrolyte so that dark currents electrochemically driven should decrease. The DSSC treated with three cycles of alumina (AAA) therefore shows the smallest dark current, whereas the titania-coating (TTT) shows the largest.

Accelerated DSSC lifetime test was conducted using thermal aging for 500 h in the dark at 80°C, where device performance was monitored every 100 h. These conditions are normally used to quantify thermal stability of DSSCs.[42,43] Results of best treated DSSC (TAA and AAT) including control are shown in Figure 5. For the control DSSC, overall power conversion efficiency drops within the first 200 h and saturates at ~4.4 %, or about 40% less than the initial performance. This result is comparable to a previous report by Grätzel and co-workers who found ~43% efficiency loss under same conditions.[44] ALD treated DSSCs perform much better in these lifetime tests as seen in Figure 5(a). Figure 5(b) clearly shows that the best performers, TAA and AAT, maintain 83% and 86% of their initial performance respectively and more impressive is that after 250 h, both of these cells show an overall efficiency >5.1%, which is >14% larger than the control device (~4.4%). Figure S10 indicates that the rest of ALD treatments also maintain about 80% of their initial efficiencies. From the data in Figures S10 we conclude that the degraded efficiency is most closely related to a decrease in J_{sc}, which is well known to be linked to dye desorption during thermal aging. Collectively, the data presented here provides strong evidence that ultra-thin ALD coatings with multicomponent applied to photoanodes after dye sensitization improve dye-attachment in functioning DSSC devices.

Considering the nucleation and growth of ALD at early stage, three cycle of ALD Al_2O_3 and TiO_2 used here will not form a continuous film on N719.[41,45,46] Instead, it is likely that three cycles of Al_2O_3 and TiO_2 will form a composite oxide on TiO_2-N719 modifying binding between dye and TiO_2. This is consistent with TAA and AAT showing similar performance for dye stabilization, DSSC performances, and thermal stability. The Al_2O_3:TiO_2 2:1 ratio can enhance electronic coupling between the dye and the TiO_2 conduction band, providing better performance than the ALD TiO_2 or Al_2O_3 alone for N719.

4. Conclusion

In summary, we have presented the first study using mixed ALD layers to stabilize N719 dye molecules in DSSCs and extend their useful lifetimes. These improvements employed subnanometer layers of oxide materials applied after dye-sensitization. Applying these layers while still maintaining high performance devices remains a challenge. However, in this work, we demonstrate that mixed ALD of Al_2O_3 and TiO_2 can give devices with 90% of the performance of untreated DSSCs and significantly extended lifetimes. Based on *in situ* IR spectroscopy we partially attribute this improvement to an increase in carboxylate binding strength

upon ALD treatment. However, these IR studies also reveal that ALD precursors may react with NCS ligands on the N719 dye, possibly causing the reduction in initial DSSSC performance. Nevertheless, this work successfully demonstrates that ALD is a very powerful strategy for stabilizing dye molecules on mesoporous metal oxide surfaces used in device structures. Large opportunity exists in further optimizing dye molecule structure, metal precursor reactivity, and ALD reaction conditions to meet or exceed untreated DSSC designs.

Acknowledgements

D.H.K. acknowledges support from U.S. Department of Energy Project #:8NT0001925. K.H. and L.A acknowledge support from the UNC Energy Frontier Research Center (EFRC) "Center for Solar Fuels", an EFRC funded by the U.S. Department of Energy, Office of Science, and Office of Basic Energy Sciences under award DE-SC0001011. Support for M.K.L. was provided by the Research Triangle Solar Fuels Institute.

Notes and references

[a] Department of Chemical and Biomolecular Engineering, North Carolina State University, 911 Partners Way, Campus Box 7905, Raleigh, NC 27695, USA

[b] Department of Chemistry, University of North Carolina at Chapel Hill, 123 South RD, Chapel Hill, NC, 27599-3290, USA

* E-mail: gnp@ncsu.edu

† Electronic Supplementary Information (ESI) available: See DOI: 10.1039/b000000x/

1. B. O'Regan and M. Grätzel, *Nature*, 1991, **353**, 737–740.
2. A. Yella, H.-W. Lee, H. N. Tsao, C. Yi, A. K. Chandiran, M. K. Nazeeruddin, E. W.-G. Diau, C.-Y. Yeh, S. M. Zakeeruddin, and M. Grätzel, *Science*, 2011, **334**, 629–634.
3. M. I. Asghar, K. Miettunen, J. Halme, P. Vahermaa, M. Toivola, K. Aitola, and P. Lund, *Energy Environ. Sci.*, 2010, **3**, 418–426.
4. H.-J. Son, C. Prasittichai, J. E. Mondloch, L. Luo, J. Wu, D. W. Kim, O. K. Farha, and J. T. Hupp, *J. Am. Chem. Soc.*, 2013, **135**, 11529–11532.
5. E. Figgemeier and A. Hagfeldt, *Int. J. Photoenergy*, 2004, **6**, 127–140.
6. H. T. Nguyen, H. M. Ta, and T. Lund, *Sol. Energy Mater. Sol. Cells*, 2007, **91**, 1934–1942.
7. K. Hanson, M. K. Brennaman, H. Luo, C. R. K. Glasson, J. J. Concepcion, W. Song, and T. J. Meyer, *ACS Appl. Mater. Interfaces*, 2012, **4**, 1462–1469.
8. C. Yoshida, S. Nakajima, Y. Shoji, E. Itoh, K. Momiyama, K. Kanomata, and F. Hirose, *J. Electrochem. Soc.*, 2012, **159**, H881–H884.
9. P. Wang, C. Klein, R. Humphry-Baker, S. M. Zakeeruddin, and M. Grätzel, *Appl. Phys. Lett.*, 2005, **86**, 123508–123508–3.
10. P. Wang, S. M. Zakeeruddin, R. Humphry-Baker, J. E. Moser, and M. Grätzel, *Adv. Mater.*, 2003, **15**, 2101–2104.
11. J. Lim, Y. S. Kwon, S.-H. Park, I. Y. Song, J. Choi, and T. Park, *Langmuir*, 2011, **27**, 14647–14653.
12. J. Lim, Y. S. Kwon, and T. Park, *Chem. Commun.*, 2011, **47**, 4147–4149.
13. N. Heo, Y. Jun, and J. H. Park, *Sci. Rep.*, 2013, **3**, 1–6.
14. S.-H. Park, J. Lim, I. Y. Song, N. Atmakuri, S. Song, Y. S. Kwon, J. M. Choi, and T. Park, *Adv. Energy Mater.*, 2012, **2**, 219–224.
15. R. Harikisun and H. Desilvestro, *Sol. Energy*, 2011, **85**, 1179–1188.
16. A. Hinsch, J. M. Kroon, R. Kern, I. Uhlendorf, J. Holzbock, A. Meyer, and J. Ferber, *Prog. Photovolt. Res. Appl.*, 2001, **9**, 425–438.
17. G. N. Parsons, S. M. George, and M. Knez, *MRS Bull.*, 2011, **36**, 865–871.
18. A. B. F. Martinson, J. W. Elam, J. T. Hupp, and M. J. Pellin, *Nano Lett.*, 2007, **7**, 2183–2187.
19. M. Law, L. E. Greene, A. Radenovic, T. Kuykendall, J. Liphardt, and P. Yang, *J. Phys. Chem. B*, 2006, **110**, 22652–22663.
20. K. Park, Q. Zhang, B. B. Garcia, X. Zhou, Y.-H. Jeong, and G. Cao, *Adv. Mater.*, 2010, **22**, 2329–2332.
21. A. B. F. Martinson, J. W. Elam, J. Liu, M. J. Pellin, T. J. Marks, and J. T. Hupp, *Nano Lett.*, 2008, **8**, 2862–2866.
22. D. H. Kim, M. Woodroof, K. Lee, and G. N. Parsons, *ChemSusChem*, 2013, **6**, 1014–1020.
23. M. D. Losego and K. Hanson, *Nano Energy*, 2013, **2**, 1067–1069.
24. K. Hanson, M. D. Losego, B. Kalanyan, D. L. Ashford, G. N. Parsons, and T. J. Meyer, *Chem. Mater.*, 2013, **25**, 3–5.
25. B. Gong and G. N. Parsons, *J. Mater. Chem.*, 2012, **22**, 15672–15682.
26. G.-W. Lee, D. Kim, M. J. Ko, K. Kim, and N.-G. Park, *Sol. Energy*, 2010, **84**, 418–425.
27. J. M. Ball, M. M. Lee, A. Hey, and H. J. Snaith, *Energy Environ. Sci.*, 2013, **6**, 1739–1743.
28. B. Gong, Q. Peng, and G. N. Parsons, *J. Phys. Chem. B*, 2011, **115**, 5930–5938.
29. K. S. Finnie, J. R. Bartlett, and J. L. Woolfrey, *Langmuir*, 1998, **14**, 2744–2749.
30. V. Shklover, Y. E. Ovchinnikov, L. S. Braginsky, S. M. Zakeeruddin, and M. Grätzel, *Chem. Mater.*, 1998, **10**, 2533–2541.
31. M. K. Nazeeruddin, R. Humphry-Baker, P. Liska, and M. Grätzel, *J. Phys. Chem. B*, 2003, **107**, 8981–8987.
32. G. B. Deacon and R. J. Phillips, *Coord. Chem. Rev.*, 1980, **33**, 227–250.
33. P. Wang, C. Klein, R. Humphry-Baker, S. M. Zakeeruddin, and M. Grätzel, *J. Am. Chem. Soc.*, 2005, **127**, 808–809.
34. K. Kilså, E. I. Mayo, B. S. Brunschwig, H. B. Gray, N. S. Lewis, and J. R. Winkler, *J. Phys. Chem. B*, 2004, **108**, 15640–15651.
35. J. E. Moser, D. Noukakis, U. Bach, Y. Tachibana, D. R. Klug, J. R. Durrant, R. Humphry-Baker, and M. Grätzel, *J. Phys. Chem. B*, 1998, **102**, 3649–3650.
36. K. Hanson, M. D. Losego, B. Kalanyan, G. N. Parsons, and T. J. Meyer, *Nano Lett.*, 2013, **13**, 4802–4809.
37. S. Ito, M. K. Nazeeruddin, P. Liska, P. Comte, R. Charvet, P. Péchy, M. Jirousek, A. Kay, S. M. Zakeeruddin, and M. Grätzel, *Prog. Photovolt. Res. Appl.*, 2006, **14**, 589–601.
38. T. W. Hamann, O. K. Farha, and J. T. Hupp, *J. Phys. Chem. C*, 2008, **112**, 19756–19764.
39. Y. Diamant, S. Chappel, S. G. Chen, O. Melamed, and A. Zaban, *Coord. Chem. Rev.*, 2004, **248**, 1271–1276.
40. L. J. Antila, M. J. Heikkilä, V. Aumanen, M. Kemell, P. Myllyperkiö, M. Leskelä, and J. E. I. Korppi-Tommola, *J. Phys. Chem. Lett.*, 2010, **1**, 536–539.
41. L. J. Antila, M. J. Heikkilä, V. Mäkinen, N. Humalamäki, M. Laitinen, V. Linko, P. Jalkanen, J. Toppari, V. Aumanen, M. Kemell, P. Myllyperkiö, K. Honkala, H. Häkkinen, M. Leskelä, and J. E. I. Korppi-Tommola, *J. Phys. Chem. C*, 2011, **115**, 16720–16729.
42. P. T. Nguyen, P. E. Hansen, and T. Lund, *Sol. Energy*, 2013, **88**, 23–30.
43. P. Tuyet Nguyen, A. Rand Andersen, E. Morten Skou, and T. Lund, *Sol. Energy Mater. Sol. Cells*, 2010, **94**, 1582–1590.
44. P. Wang, S. M. Zakeeruddin, J. E. Moser, M. K. Nazeeruddin, T. Sekiguchi, and M. Grätzel, *Nat. Mater.*, 2003, **2**, 402–407.
45. T.-C. Tien, F.-M. Pan, L.-P. Wang, F.-Y. Tsai, and C. Lin, *J. Phys. Chem. C*, 2010, **114**, 10048–10053.
46. U. Terranova and D. R. Bowler, *J. Phys. Chem. C*, 2012, **116**, 4408–4415.